

## Corrosion behavior of PCB-ENIG in a simulated marine atmospheric environment with industrial pollution

Kai Zhang<sup>1,3</sup>, Bangwei Wen<sup>1</sup>, Lunwu Zhang<sup>1</sup>, Chao Li<sup>1</sup>, Jun Liu<sup>1</sup>, Pan Yi<sup>2,\*</sup>

<sup>1</sup>Southwest Technology and Engineering Research Institute, Chongqing 400039, China

<sup>2</sup> Key Laboratory for Corrosion and Protection (MOE), Institute for Advanced Materials and Technology, University of Science and Technology Beijing, Beijing 100083, China

<sup>3</sup>Wanning Hainan, Materials Corrosion in Atmospheric Environment, National Observation & Research Station, Hainan 571522, China

\*E-mail: [bkyipan@126.com](mailto:bkyipan@126.com)

Received: 9 June 2020/ Accepted: 23 August 2020 / Published: 30 September 2020

---

In this work, the corrosion behavior of printed circuit board finished with electroless nickel immersion gold (PCB-ENIG) in a simulated marine atmospheric environment with industrial pollution is studied through corrosion topography observation, electrochemical measurement and surface Kelvin potential analysis. The results show that at the initial stage, micropores corrosion is the main damage formation for PCB-ENIG. However, the initial corrosion products accumulate on the sample surface and block the micropores, restrict the infiltration process of chloride ions and hydrogen ions. Therefore, the surface Kelvin potential and electron transfer resistance increase at initial stage. As the extending of exposure time, some localized corrosion products shed off due to the crack initiation, resulting in the direct exposure of substrate Cu to the acid salt spray environment. Consequently, the coating loses the protection effects on Cu.

---

**Keywords:** PCB-ENIG, Micropores corrosion, Marine atmospheric environment, Industrial pollution, Surface Kelvin potential

### 1. INTRODUCTION

In recent decades, the electronic components are developing toward miniaturization and highly integrated direction due to the requirement of portable and multi-functional products [1, 2]. The trade-off for this technological improvement is that the parts (eg, printed circuit boards, PCBs) in electronic equipments are becoming more sensitive to contaminants so that they are more prone to suffer from corrosion failure. The previous studies also pointed out that the trace of pollutants can threaten significantly the reliability and the service life of electronic devices [3, 4], and the maximum allowable pollutant concentration for electronic components is even less than it for maintaining human health.

For example, the highest allowable concentration of H<sub>2</sub>S for human health and electronic components is 10000 ppbv and 10 ppbv, respectively [5, 6].

To improve the wettability and corrosion resistance, some surface treatments, such as organic solderability, electroless nickel/immersion gold treatment (ENIG), lead-free tin hot air leveling (HASL), immersion silver (ImAg) and so on, are applied on PCBs [7-10]. Among them, ENIG surface finish includes an intermediate Ni layer and a thin Au layer on copper substrate. However, in recent years, more and more devices are applied in the harsh environment, for example marine and industrial polluted atmospheric environment. In these situations, the printed circuit boards with surface treatment still suffer from significant corrosion damage and finally decrease its service life. Ambat[11] investigated the corrosion mechanism of dome (Ag/AISI 202 steel) and key pad system (Au/Ni/Cu) in mobile phone in the chloride-containing environment and the results suggested that the pad and dome surface displayed obvious localized corrosion damage and the pitting corrosion extended to the underlying metal. Then Salahinejad [12] reported the galvanic-pitting corrosion of copper electrical pads treated with ENIG surface finish in a sulfur-containing humid atmosphere. The results indicated that mainly the Cu substrate and slightly the Ni interlayer underwent the corrosion damage and the synergistic galvanic pitting corrosion event was responsible for this attack. However, to the best of our knowledge, the synergistic effects of multi-factors on the corrosion behavior of PCB-ENIG are still lacked.

In this work, an acid salt-spray experiment (the environment containing Cl<sup>-</sup> and SO<sub>2</sub>) are conducted for PCB-ENIG to simulate the polluted marine atmosphere service environment. Stereo microscope and environment scanning electron microscope (SEM) with an energy dispersive spectrometer (EDS) are used to observe the corrosion topographies and the composition of corrosion products. The electrochemical impedance spectroscopy (EIS), and a scanning Kelvin probe (SKP) were applied to analyze the corrosion failure mode and mechanism of PCB-ENIG samples. This work can provide the data support and guidance for the selection for PCB usage under the polluted marine atmospheric environment and also enriches the corrosion theory of PCB-ENIG in atmospheric environment.

## **2. EXPERIMENTAL**

### *2.1 Materials and methods*

PCB-ENIG specimens with 0.02 μm thick Au layer are used for the experiments. Before the acid salt-spray experiments, PCB-ENIG samples are ultrasonically cleaned with acetone and deionized water for 10 min in sequence and then air-dried using a cold air from hair dryer. After pre-treatment, these samples are placed into a home-made box, the detailed layout can refer to Ref. [13]. Then this box is placed into a salt spray chamber (CCX2000). For the salt spray experiment, the temperature is 35°C and the concentration of NaCl in the chamber is 5wt.%. And SO<sub>2</sub> is continuously bubbled into the chamber. After exposure for 16 h, 24 h, 48 h, 96 h and 168 h, respectively, the PCB-ENIG samples are retrieved and washed slightly using deionised water and then dried for further analysis.

## 2.2 Corrosion morphology observation and composition analysis

Stereo microscopy (Keyence VHX-2000) and environment SEM (ESEM, FEI Quanta 250) with an energy dispersive spectrometer (EDS) were employed to observe the corrosion morphology and analyze the composition of corrosion product.

## 2.3 Electrochemical measurements

EIS measurements were conducted for the retrieved samples in a conventional three-electrode system using the PARSTAT 2273 electrochemical workstation. A platinum foil was used as counter-electrode and a saturated calomel electrode was used as reference electrode. EIS measurements were performed at open-circuit potential with a perturbation of 10 mV and measuring frequency range of 100 kHz to 10 mHz. All the electrochemical measurements were repeated for three times at least. ZSimpWin V3.20 software was applied for EIS data fitting.

## 2.4 Surface Kelvin potential tests

The surface Kelvin potential of a sample surface is measured using M370SKP with a work distance of  $100 \pm 2 \mu\text{m}$  and step size of  $100 \mu\text{m}$ . All experiments were conducted in the room temperature environment.

# 3. RESULTS AND DISCUSSION

## 3.1 Morphology analyses of the specimens

Fig.1 shows the optical micrographs of PCB-ENIG exposed in the salt spray chamber for different periods. It can be observed that the PCB-ENIG surface (blank sample) is smooth before the salt spray experiment. After immersion in the salt spray chamber for 16 h, a slight amount of pits distribute on the surface of PCB-ENIG (Fig.1b), indicating pitting corrosion caused by micropores is the main damage formation for PCB-ENIG under the environment containing chloride and  $\text{SO}_2$ . As the time elapses, the size and amount of pits increase (Fig.1c). After 48 h, some green corrosion products emerge on the sample surface and continuously increase with the extending of exposure time. When the exposure time reaches 168 h, the green corrosion products almost cover the entire sample surface.

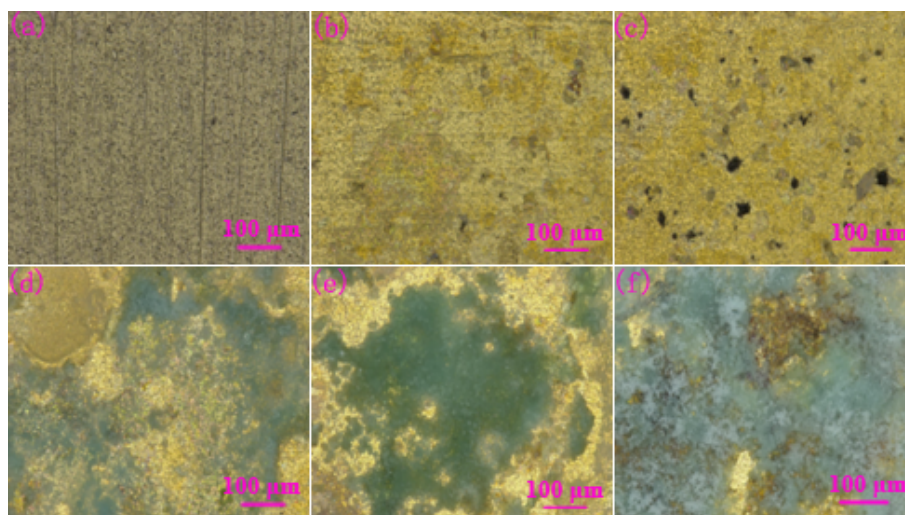


**Figure 1.** The optical micrographs of PCB-ENIG after different periods of exposure ( $\times 300$ ): (a) 0 h; (b) 16 h; (c) 24 h; (d) 48 h; (e) 96 h; (f) 168 h

To further inspect the corrosion behavior change law of PCB-ENIG in salt spray environment containing  $\text{SO}_2$ , the micro-topographies of PCB-ENIG are obtained by SEM, as is shown in Fig.2. It can be seen that PCB-ENIG sample suffers from serious local corrosion after 16 h (Fig.2b). In addition, some microcracks are progressively formed on the corrosion products surface. As the salt spray time extends, the corrosion aggravates and a lot of corrosion products cover on the PCB-ENIG surface. Even local protective coating shed off and the substrate is exposed (Fig.2f). It is noteworthy that many pits can be obviously found on the substrate surface, which indicates that Cu undergoes pitting corrosion. And the corrosion products gradually migrate to the samples surface, thus the surface corrosion products exhibit green color, which is consistent with the optical micrographs.

EDS is used to analyze the composition of corrosion products, as is shown in Table 1. It can be found that the corrosion products in area A and B contain element Cl, and the atomic ratio of Cu/Cl is around 2: 1 for the corrosion products in area A. Moreover, the corrosion products display green color according to the optical micrographs. Thus it can be speculated that the corrosion products include  $\text{Cu}_2\text{Cl}(\text{OH})_3$  [14]. Compared with area A, element Cu and O content in corrosion products at area B is much higher, indicating that the corrosion extent of PCB-ENIG aggravates significantly with the extending of exposure time. Moreover, the EDS result of area C displays that there are lots of element Cu and the amount of element Ni is relative small. This is mainly because the surface coating (Ni and Au layer) gradually shed off due to the effects of serious corrosion and cracks after 168 h salt spray experiments, resulting in the direct exposure of Cu substrate to the atmospheric environment. On the other hand, compared with area C, the area B includes more Ni and a certain amount of Cu, which further implies that the pitting corrosion is the main damage formation for PCB-ENIG and the corrosion products of Cu substrate migrate outside through the micropores and finally accumulates on the sample surface.

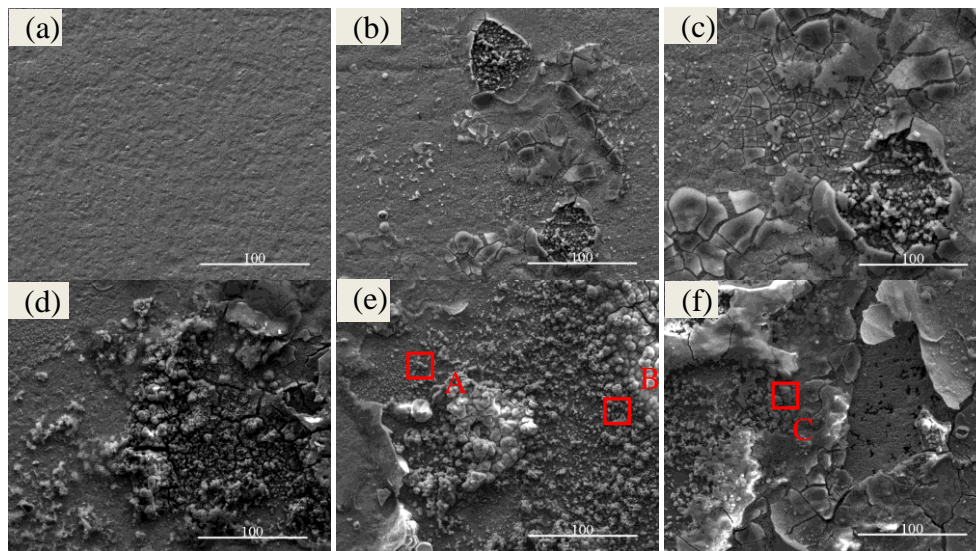


**Figure 2.** The micro-topographies of PCB-ENIG after different experiment periods: (a)0 h; (b)16 h; (c)24 h; (d)48 h; (e)96 h; (f)168 h

**Table 1.** The EDS analysis results of the corrosion products (At%)

Element	C	O	S	P	Cl	Ni	Cu	Au
Area A	7.66	29.04	0.15	4.06	6.51	36.69	11.42	4.48
Area B	4.92	39.20	0.08	7.05	5.61	23.72	18.19	1.22
Area C	1.96	6.41	0.64	0.93	0.53	1.87	85.87	1.78

### 3.2 EIS analysis

To investigate the interfacial reactions of PCB-ENIG exposed for different periods in acid salt spray environment and the protection effects of corrosion products on PCB-ENIG, EIS measurements are carried out and the corresponding results are shown in Fig.3. For the PCB-ENIG samples, the corrosion products covered on the surface will cause another relaxation process besides the electrochemical reactions occurred at electric double layer. Thus the EIS data of PCB-ENIG should contain two time constant. The equivalent circuit shown in Fig.4 is used to fit the EIS data [15, 16].  $R_s$  represents the solution resistance.  $Q_f$  and  $R_f$  are related to corrosion products layer.  $Q_{dl}$  and  $R_{ct}$  correspond to the electric double layer capacitance and the charge transfer resistance. For the constant phase element  $Q$ ,

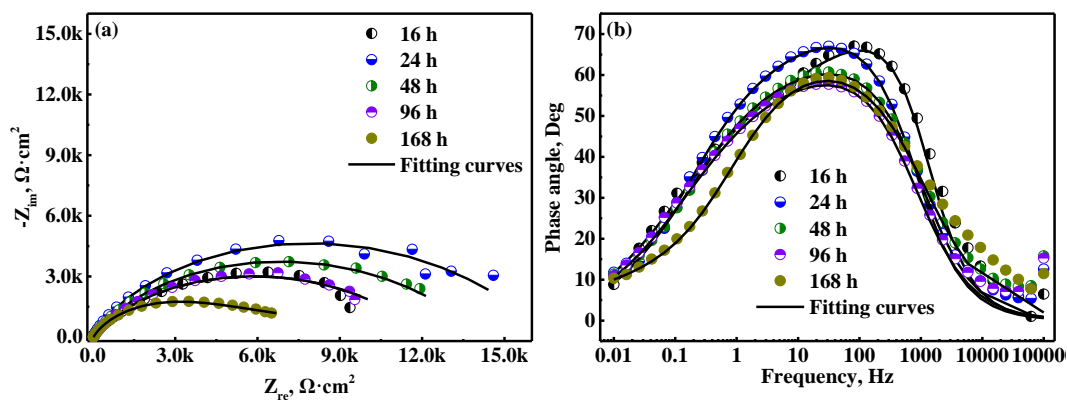
$$Z_{CPE} = \frac{1}{Y_0(j\omega)^n} \quad (1)$$

where  $\omega$  represents the angular frequency (Hz);  $Y_0$  is the ideal capacitance (F);  $n$  is the exponent and varies between 0 and 1. When the value of  $n$  is 1, 0.5 and 0,  $Q$  represents ideal capacitor, Warburg impedance and ideal resistor, respectively. For the situation of  $n=-1$ ,  $Q$  describes the inductive behavior [17, 18].

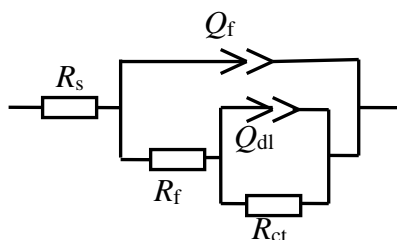
Table 2 displays the fitted results of EIS data. It can be seen that as the exposure time extends,

the corrosion products resistance ( $R_f$ ) gradually increases. Especially, the  $R_f$  value of sample after 168 h is much higher than the other periods. This phenomenon can be explained as follow: at the early and stages of the test, PCB-ENIG just suffers from slight corrosion and the corrosion products covered on the surface is very small, thus the corrosion products resistance is small. As the extending of exposure time, the corrosion products increases and so the  $R_f$  value enhances, which agrees with the optical micrographs well. It is noteworthy that after 168 h salt spray experiment, a large number of coating detach from the Cu substrate due to the effects of corrosion. In this situation, in fact,  $R_f$  includes the resistance of the remaining coating besides the corrosion products resistance, thus  $R_f$  shows a sharp increase trend after 168 h.

$R_{ct}$  represents the resistance of electron transfer process at electric double layer, thus it can be applied to evaluate the corrosion resistance of materials [19, 20]. The larger the  $R_{ct}$  value, the better the corrosion resistance. In this work, the  $R_{ct}$  value of PCB-ENIG from EIS fitting using the equivalent circuit in Fig.4 is shown in Fig.5. It can be seen that the  $R_{ct}$  value is very small at the initial stage. As the acid salt spray experiment time elapses,  $R_{ct}$  value gradually increases. When the time exceeds 24 h, the  $R_{ct}$  value starts to decrease again. This phenomenon can be explained as follow. The Au layer is very thin, thus there are inevitably some micropores on the sample surface [21, 22]. At the initial stage, the acid electrolyte containing chloride ions continuously penetrate into the micropores and cause the Ni and Cu layer corrosion. Moreover, the micro-galvanic couples between Au and Ni, Cu will also accelerate the substrate corrosion [23]. Consequently, the initial corrosion rate is great, that is, the  $R_{ct}$  value is relatively small.



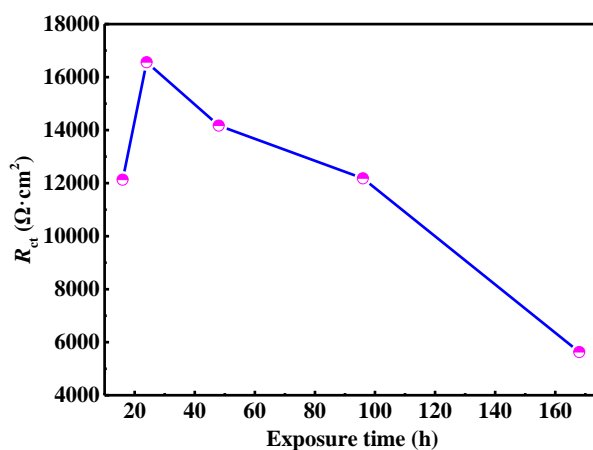
**Figure 3.** Nyquist (a) and Bode phase angle (b) plots of PCB-ENIG exposed for different periods in acid salt spray environment



**Figure 4.** The equivalent circuit for EIS data fitting

**Table 2.** EIS fitting results of PCB-ENIG after the salt spray tests for different periods

Time, h	$R_s$ , $\Omega \cdot \text{cm}^2$	$CPE_f$ $\text{S} \cdot \text{s}^n \cdot \text{cm}^{-2}$	n	$R_f$ , $\Omega \cdot \text{cm}^2$	$CPE_{dl}$ $\text{S} \cdot \text{s}^n \cdot \text{cm}^{-2}$	n	$R_{ct}$ , $\Omega \cdot \text{cm}^2$
16	20.41	1.083E-5	1	64.42	1.219E-4	0.5603	1.213E4
24	21.68	1.596E-5	0.9379	72.42	6.267E-5	0.5852	1.656E4
48	26.7	1.701E-5	0.886	82.97	7.467E-5	0.5625	1.417E4
96	29.97	2.305E-5	0.8589	90.31	9.514E-5	0.5269	1.218E4
168	22.03	6.88E-5	0.7303	4106	4.941E-4	0.3763	5.627E3

**Figure 5.** Time dependence of  $R_{ct}$  value under different acid salt spray experiment period

As the acid salt spray experiment time extends, the corrosion products gradually accumulate on the sample surface. In fact these corrosion products block the micropores on the surface and thus restrict the substrate corrosion process to some extent. So, the  $R_{ct}$  value gradually increases as the time extends. However, the PCB-ENIG suffers from serious corrosion and many cracks occur on the corrosion products surface after 24 h. Moreover, 96 h later, some local area Ni layer sheds off and loses the protection function. In this situation, the Cu substrate directly contact with acid electrolyte containing chloride ions. Therefore, at the later stage of acid salt spray experiment, the  $R_{ct}$  value sharply decreases.

### 3.3 Surface Kelvin potential tests

To investigate the corrosion behavior law of PCB-ENIG under acid salt spray environment, the surface Kelvin potential of PCB-ENIG samples experienced acid salt spray tests are obtained through SKP experiments, as is shown in Fig.6. Table 3 and Fig.7 shows the Gaussian fitting results of surface Kelvin potential. The previous studies indicated that the corrosion potential commonly has linear relationship with surface Kelvin potential [24-26]. Thus surface Kelvin potential can be used to thermodynamically evaluate the corrosion resistance. It can be seen from Fig.6 and Fig.7 that the Kelvin potential gradually enhances at the initial stage and then shows a descending trend with the increasing of acid salt spray experiments. This is mainly because the micro-pore corrosion occurred for PCB-ENIG in the early stage of the test, and the corrosion products continuously accumulated in the

micro-pores, which hindered the escape process of the electrons on the surface of the sample. Thus the surface Kelvin potential increases and the entire potential map develops a warm tone. On the other hand, the oxidation of substrate metals is accompanied by the volume expansion and development of compressive stress due to the molar volume difference between metal and the oxides, and thus leading to the initiation of micro-cracks and the corrosion products shedding off. In this situation, the substrate Cu is directly exposed to the acid salt spray environment, which makes the electron escape process easier. Consequently, at later stage of acid salt spray experiment, the surface potential of PCB-ENIG decreases, and the corrosion tendency increases. Moreover, it can be found from Fig.6e that the local area on PCB-ENIG surface shows the cold tone, indicating that the surface Kelvin potential is small and this is resulting from the micropores corrosion and corrosion products shedding off. This phenomenon is also agreement with the surface micro-topogaphies in Fig.2. In addition, Table 3 also shows the fitting standard deviation  $\sigma$  initially decreases and then increases, which suggests that the distribution of surface Kelvin potential of PCB-ENIG at the later stage is very uneven due to local corrosion products shedding off. In fact, it further aggravates the micro-galvanic couple effects.

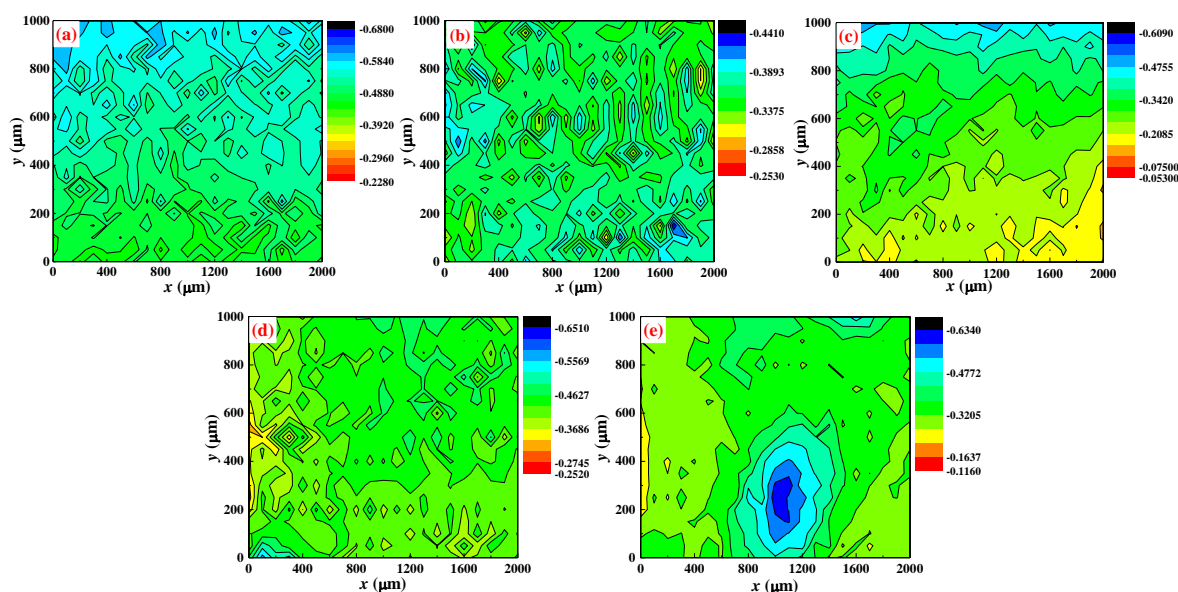


**Figure 6.** The surface Kelvin potential mapping of PCB-ENIG experienced different time acid salt spray tests: (a)16 h; (b)24 h; (c)48 h; (d)96 h; (e)168 h

**Table 3.** The Gaussian fitting results of Surface Kelvin potential

	16 h	24 h	48 h	96 h	168 h
$\mu/V$	-0.5225	-0.3645	-0.2804	-0.3299	-0.4338
$\sigma$	0.05018	0.02747	0.02108	0.03738	0.06888

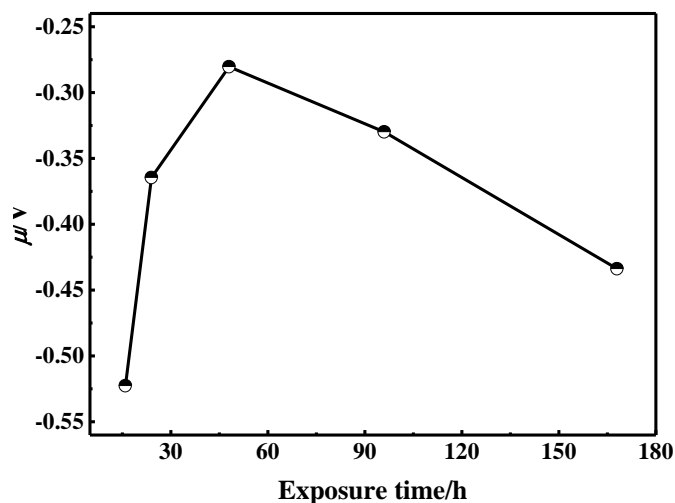


**Figure 7.** The relationship curves of SKP expectation vs. exposure time

### 3.4 Corrosion failure mechanism

For PCB-ENIG, as we know, it is inevitable that there is presence of some micropores on the surface due to the extreme thin Au layer. Upon exposure to the salt spray environment, the thin electrolyte layer is formed on the PCB-ENIG surface. When  $\text{SO}_2$  is pumped into the salt spray chamber, the  $\text{SO}_2$  molecules will be absorbed and solvated in the thin electrolyte layer. This will cause a slight acidification of the thin electrolyte layer [27]. The acid environment can induce the dissolution of the passive film covered on Ni and Cu surface and thus decrease the stability. On the other hand, chloride ions and hydrogen ions infiltrate into the micropores and lead to the electrochemical corrosion dissolution of Ni and Cu layer. Moreover, the corrosion potential of Au layer is much higher than Ni and Cu and thus the micro-galvanic couples are formed, which also significantly accelerates the corrosion process of Ni and Cu [11, 12, 23]. It is noteworthy that at the initial stage, the corrosion products accumulate on the PCB-ENIG surface and block the infiltration process of chloride ions and hydrogen ions. Thus the initial corrosion products have protection effects on the PCB-ENIG samples, which is also confirmed by EIS and Kelvin potential tests results. The corrosion process of substrate metals is accompanied by the volume expansion due to the molar volume difference between metal and the oxides. Consequently, some cracks emerge and even the local corrosion products shed off at the later period. The coating almost loses the protection function.

## 4. CONCLUSIONS

In this work, the corrosion behavior of PCB-ENIG in marine environment with industrial pollution is studied by the acid salt spray experiment in connection of surface topography observation, electrochemical measurement and surface Kelvin potential tests. In the acid salt spray environment, the thin electrolyte layer containing chloride ions is acidic due to the dissolution of  $\text{SO}_2$ , which will induce the dissolution of the passive film covered on Ni and Cu layer and further cause their electrochemical

corrosion. On the other hand, the corrosion potential of Au is much higher than Ni and Cu, thus the micro-galvanic couples between Au and Ni, Cu are formed and further accelerates the electrochemical corrosion process. Overall, the pitting corrosion resulting from the micropores corrosion is the main failure mechanism for PCB-ENIG.

## References

1. P. Yi, K. Xiao, K. Ding, G. Li, C.F. Dong, X.G. Li, *T. Nonferr. Metal Soc.*, 26 (2016) 1146.
2. A. Khangholi, R.I. Revilla, A. Lutz, S. Loulidi, E. Rogge, G.V. Assche, I.D. Graeve, *Prog. Org. Coat.*, 137 (2019) 105256.
3. P. Yi, C.F. Dong, K. Xiao, X.G. Li, *Appl. Surf. Sci.*, 399 (2016) 608.
4. T.H. Tseng, A.T.J.M.R. Wu, *Microelectron. Reliab.*, 98 (2019) 19.
5. S. Zou, X.G. Li, C.F. Dong, K. Ding, K. Xiao, *Electrochim. Acta*, 114 (2013) 363.
6. C. Leygraf, I.O. Wallinder, J. Tidblad, T. Graedel, *Atmospheric corrosion*, John Wiley & Sons, 2016.
7. B.K. Kim, S.J. Lee, J.Y. Kim, K.Y. Ji, Y.J. Yoon, M.Y. Kim, S.H. Park, J.S. Yoo, *J. Electron. Mater.*, 37 (2008) 527.
8. D.J. Lee, S.H. Huh, C.S. Kim, S. Mun, H.K. Shin, H.J. Lee, *Electron. Mater. Lett.*, 11 (2015) 695.
9. K.K. Ding, X.G. Li, K. Xiao, C.F. Dong, K. Zhang, R.T. Zhao, *T. Nonferr. Metal Soc.*, 25 (2015) 2446.
10. M. Baciór, N. Sobczak, A. Siewiorek, A. Kudyba, M. Homa, R. Nowak, M. Dziula, S. Masłoń, *J. Mater. Eng. Perform.*, 24 (2015) 754.
11. R. Ambat, P. Møller, *Corros. Sci.*, 49 (2007) 2866.
12. E. Salahinejad, R.E. Farsani, L.J.E.F.A. Tayebi, *Eng. Fail. Anal.*, 77 (2017) 138.
13. L. Yan, K. Xiao, P. Yi, C. Dong, J. Wu, C. Mao, X.G. Li, *J. Alloy Compd.*, 688 (2016) 301.
14. E.J. Schindelholz, H. Cong, C.F. Jove-Colon, S. Li, J.A. Ohlhausen, H.K. Moffat, *Electrochim. Acta*, 276 (2018) 194.
15. P. Yi, C.F. Dong, K. Xiao, C. Man, X.G. Li, *J. Electroanal. Chem.*, 809 (2018) 52.
16. E.H. Saarivirta, P. Rajala, M. Bomberg, L. Carpén, *Electrochim. Acta*, 240 (2017) 163.
17. J.M. Vega, S. Chimentí, E. García-Lecina, H.J. Grande, M. Paulis, J.R. Leiza, *Prog. Org. Coat.*, 148 (2020) 105706.
18. R.I. Revilla, B. Wouters, F. Andreatta, A. Lanzutti, L. Fedrizzi, I.D. Graeve, *Corros. Sci.*, 167 (2020) 108480.
19. X. Dong, Q. Sun, Y. Zhou, Y. Qu, H. Shi, B. Zhang, S. Xu, W. Liu, N. Li, J. Yan, *Corros. Sci.*, 170 (2020) 108688.
20. L. Guo, F. Zhang, L. Song, R.C. Zeng, S.Q. Li, E.H. Han, *Surf. Coat. Tech.*, 328 (2017) 121.
21. I. Notter, D. Gabe, *Corros. Rev.*, 10 (1992) 217.
22. B.K. Kim, S.J. Lee, J.Y. Kim, K.Y. Ji, Y.J. Yoon, M.Y. Kim, S.H. Park, J.S. Yoo, *J. Electron. Mater.*, 37 (2008) 527.
23. E.F. Monlevade, I.A.P. Cardoso, E.F.L. Maciel, N. Alonso-Falleiros, *Eng. Fail. Anal.*, 96 (2019) 562.
24. P. Yi, K. Xiao, C. Dong, S. Zou, X. Li, *Bioelectrochemistry*, 119 (2018) 203.
25. P. Yi, K. Xiao, K. Ding, C. Dong, X. Li, *Mater. Res. Bull.*, 91 (2017) 179.
26. M. Jönsson, D. Thierry, N. LeBozec, *Corros. Sci.*, 48 (2006) 1193.
27. Q. Qu, C. Yan, Y. Wan, C. Cao, *Corros. Sci.*, 44 (2002) 2789.